

Advanced Tools for Biomechanical Modeling of the Oral, Pharyngeal, and Laryngeal Complex

2009 International Symposium on Biomechanics, Healthcare and Information Science

S. Fels¹, I. Stavness¹, A.G. Hannam², J. E. Lloyd¹, P. Anderson³, C. Batty⁴, H. Chen²,
C. Combe¹, T. Pang¹, T. Mandal¹, B. Teixeira¹, S. Green³, R. Bridson⁴, A. Lowe²,
F. Almeida², J. Fleetham⁵, R. Abugharbieh¹

¹Department of Electrical and Computer Engineering

²Faculty of Dentistry

³Department of Mechanical Engineering

⁴Department of Computer Science

⁵Department of Medicine

University of British Columbia, Vancouver, Canada

ABSTRACT

We have improved the ArtiSynth biomechanical modeling toolkit to meet new challenges in oral, pharyngeal and laryngeal modeling. Our team's current research efforts have focused on four important developments: 1. patient specific modeling, 2. updating the ArtiSynth simulation engine to support integrated soft and hard tissue models, 3. inverse modeling techniques and 4. computational fluid dynamics for air and fluid flow. We describe our progress in each of these areas along with one of our application areas: mandibular resection.

1. INTRODUCTION

Computer simulation of the oral, pharyngeal and laryngeal (OPAL) complex is becoming an increasingly useful tool for medical research, diagnosis, and treatment of conditions such as dysphagia, obstructive sleep apnea and speech disorders. For example, a 3D model of a jaw graft illustrates how a computer model may be constructed for use in understanding mastication deficits is shown in Figure 1. Effective application of computer simulation though presents many challenges require new solutions to provide methods to model specific patients' morphology, movement dynamics and disorders. These methods include new image processing techniques and medical data acquisition methods tailored to provide minimal human effort to extract OPAL morphology and dynamics. As well, providing a more powerful suite of tools to simulate both complex forward and inverse behaviours of tissue and fluids in OPAL is needed.

We have a multidisciplinary team working in each of these areas with the goals of providing new techniques for scientific study of the OPAL complex and for clinical applications in dyphagia and OSA areas. We have improved our biomechanical modeling toolkit, Artisynt to meet new challenges encountered in this research program. Our OPAL team's current research efforts have focused on four important developments: 1. patient specific modeling, 2. updating the ArtiSynth simulation engine to support integrated soft and hard tissue models, 3. inverse modeling techniques and 4. computational fluid dynamics (CFD) for air and fluid flow. We describe our progress in each of these areas and our progress on mandibular resection.

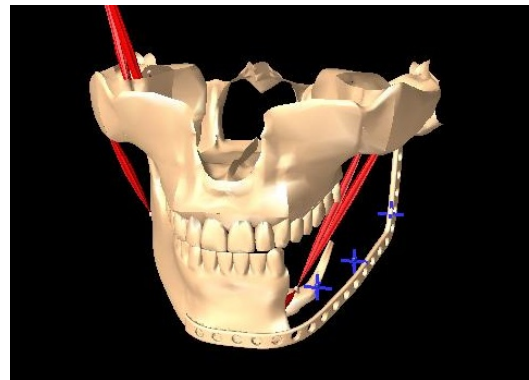


Figure 1: Generic model of a mandibular resection. The missing jaw segment has been replaced with an alloplastic reconstruction plate. Most major jaw muscles on the affected side are absent. The coordinates in blue indicate sites of arbitrary forces simulating scar components with variable stiffnesses.

2. PATIENT SPECIFIC MODELING

Our approach to patient specific modeling uses data-driven and model-driven methods to extract morphological geometry (i.e. meshes) from CT and MRI scans. We have developed oral appliances with fiducial markers for establishing rigid transformations between 3D models of dental casts and MRI scans of the OPAL region to facilitate finding tongue, palate and teeth boundaries. These markers also allow us to register sagittal, axial and coronal upper airway MRI scans to each other in order to increase the resolution of the tongue and palate volumetric structure. Using the registered scans, we use 2D and 3D live wire techniques [12] for extracting anatomical structural boundaries. Based on these boundaries, we regularize the volumes by morphing an existing tongue model [5, 24] to the extracted boundaries providing a smoother estimate of 3D meshes of OPAL structures. These meshes may then be imported into ArtiSynth for connection with other models.

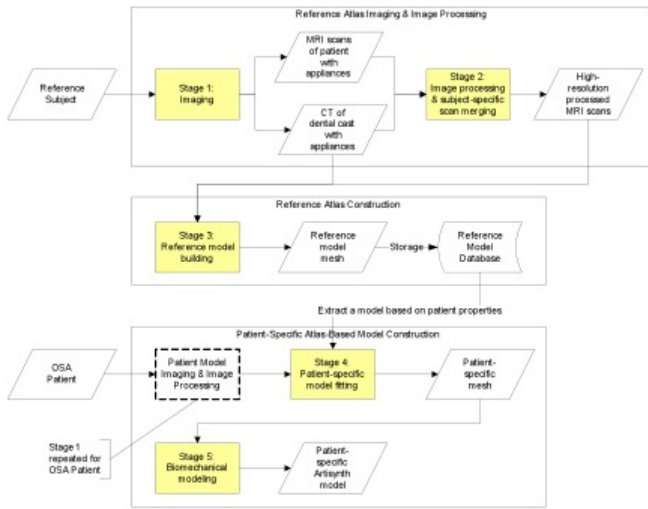


Figure 2: Workflow for patient-specific model generation.

In general, our workflow begins with data from both reference subjects and patients as shown in figure 2. Several different settings have been used during image acquisition to determine the best modality and protocols for imaging OPAL regions. Subjects wear both a protrusion oral appliance and an “at rest” oral appliance fitted with embedded fiducial markers for later registration of all the scanned images. Dental casts are made for each subject. Our MRI protocol, based on four scanned subjects, uses a Philips Achieva 3.0 Tesla MRI scanner equipped with dual coils with PD/T1-weighted images acquired with an echo time of 35ms, a repetition time of 3100 ms and a flip angle of 90°. Each volume consists of slices of 2mm thickness with 2mm spacing and in-plane resolution of 512x512 pixels. Scans were performed in three slice planes: sagittal scans with 42 slices and pixel size of 0.27x0.27 mm, coronal scans with 68 slices and pixel size of 0.32x0.32 mm, and axial scans with 84 slices and pixel size of 0.32x0.32 mm. Cone-beam CT scans are also performed on the oral appliance situated on the subject’s ceramic dental cast so that the teeth structures can be combined with the MRI data.

After the scans are completed, various image processing techniques are applied to the images to reduce the effects of noise and distortion, including: non-parametric, non-uniform intensity normalization (N3 correction) [17], cropping out the region of interest, and cubic interpolation. The three axis scans and the cone CT scan are then combined to reconstruct a single, high-resolution 3D image by registering each plane using the fiducial markers, resulting in images as shown in figures 3 and 4. We studied voxel intensity based methods using mutual information metrics [10, 23, 20], least-squares [22] approaches and robust iterated closest point (RICP) [25, 21] for effective registration. Using the fiducial markers for the process requires some human intervention to locate the centres or outlines of the markers.

This segmentation workflow has been applied to structures such as the soft palate and the tongue using different data-driven approaches. The reference models produced are then stored in a database of models for use in patient-specific model fitting. For example, figure 5 shows

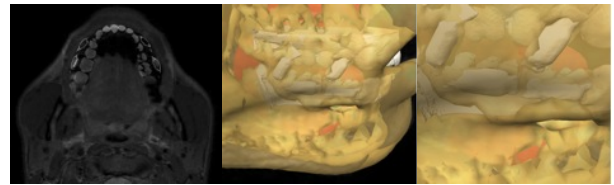


Figure 3: Combined scans used in high-resolution reconstruction: (a) Axial slice of CT with aligned MRIs combined scans, (b) Aligned surfaces extracted from scans, (c) Detail of CT markers aligned with MRI markers.

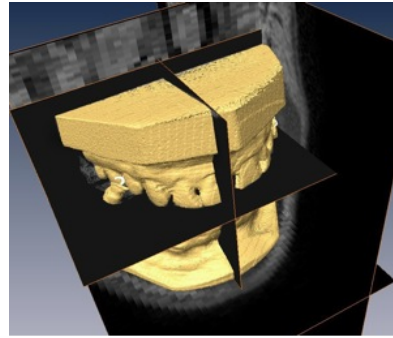


Figure 4: Registration of MRI scan to cone CT scan of dental cast.

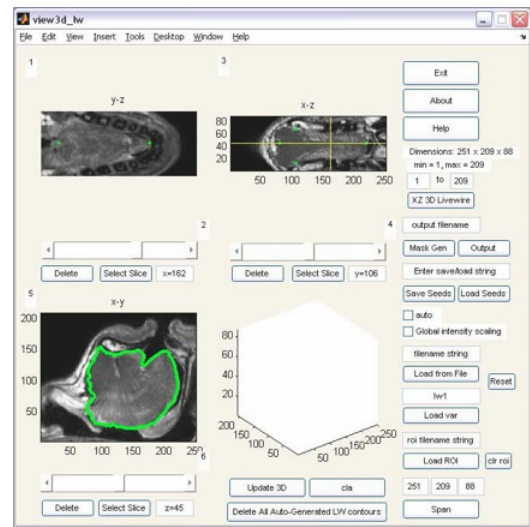


Figure 5: Segmentation of tongue using 3D Livewire interface [12].

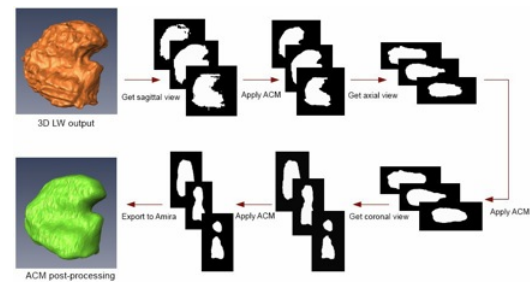


Figure 6: ACM Smoothing process applied to 3D Livewire output.

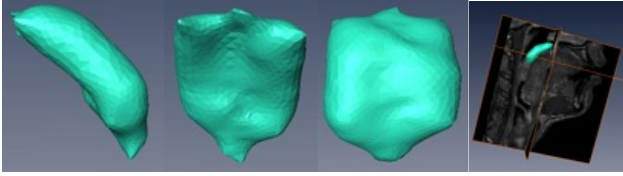


Figure 7: Soft palate surface in 3D. (a) Sagittal view, (b) Coronal view, (c) axial view. (d) Soft palate segmentation localized in the MR image space.

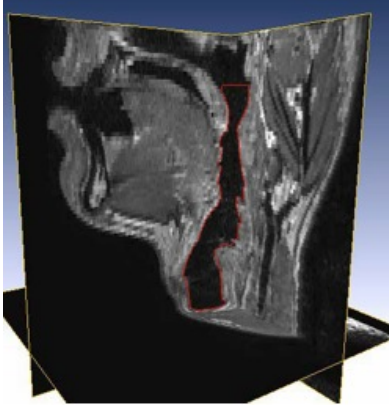


Figure 8: Segmenting the airway using Chan-Vese active contours[4].

the use of 3D Livewire [12] to segment a tongue which is then smoothed using active contour models on each 3D Livewire slice as shown in figure 6. Figure 7 shows the soft palate segmentation using the same procedure as the tongue with the final non-parallel curve networks [9] output. Figure 8 shows our approach to segmenting the vocal tract area using Chan-Vese active contours [4].

Our model-driven approach for segmenting OPAL, deforms a reference model selected from a database of models to fit the corresponding anatomical structure in a patient’s processed MRI scan. An interface allows a user to locate a landmark point on the MRI scan used to create the reference model, and its corresponding landmark point on a patient’s MRI scan. A thin-plate spline algorithm [3] is then applied to morph the reference model into a model describing the patient’s anatomy, effectively behaving like a regularizer. Accurate models with low to negligible error are generated when there is similar anatomical geometry between the atlas model and the patient MRI; however, the geometry can differ greatly among subjects, so it is necessary to have multiple reference models describing subjects that vary in body composition. We have focused our efforts using this approach on tongue modeling, however the procedure should generalize to other structures such as the soft palate. Figure 9 illustrates one of our example segmentation where the red mesh shows the original reference model and the blue mesh shows the segmentation after morphing the reference of the tongue models.

We continue to improve our methods to meet the challenges of patient specific modeling of the OPAL complex. Once the geometries are extracted we can then import them into ArtiSynth for simulation of their dynamics. Segmented tissues include both hard and soft structures and

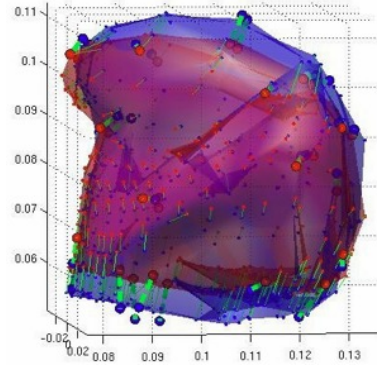


Figure 9: Overlay of reference model (red mesh) on the result from model fitting (blue mesh).

require new methods to be employed in ArtiSynth, as discussed next, for simulation fidelity appropriate for the different applications we are pursuing.

3. INTEGRATED HARD/SOFT TISSUE SIMULATION

Modeling the OPAL complex requires the combined simulation of hard and soft tissues, with collision, friction, and unilateral and bilateral constraints. We have restructured the ArtiSynth simulation engine to support fully integrated models of this kind, by formulating the dynamics as a general KKT system with inequality constraints. This is similar to the formulation described in [1], extended to handle particles and deformable body nodes as well as rigid bodies, along with constraints for deformable body contact and incompressibility. The resulting KKT system can be solved to determine the velocities at each simulation step, while an additional solve can be used to correct interpenetrations and constraint drift. In the remainder of this section we will describe the ArtiSynth simulation engine in more detail.

3.1 Integration Equations

ArtiSynth supports a number of dynamic component types, including particles, rigid bodies, and reduced coordinate models. Every dynamic component maintains a state consisting of generalized position and velocity coordinates. Particles have three degrees of freedom describing their position in space, rigid bodies have six degrees of freedom describing their position and orientation, and reduced coordinate models have r degrees of freedom describing the amplitudes of their basis functions. The combined states of all these components is collected into composite vectors of positions \mathbf{q} and velocities \mathbf{u} .

ArtiSynth also supports a number of components which are responsible for effecting forces, including axial point-to-point springs, 6D frame-to-frame springs, and finite elements (which can be thought of as volumetric springs exerting forces on their nodes). These, along with external forces such as gravity, are combined into a composite force vector $\mathbf{f}(\mathbf{q}, \mathbf{u}, t)$ which is a function of position, velocity, and time. In addition to forces, the system also provides bilateral constraints $\mathbf{G}(\mathbf{q})\mathbf{u} = 0$, which include rigid body joints and deformable model incompressibility (currently implemented using [8]), as well as unilateral constraints $\mathbf{N}(\mathbf{q})\dot{\mathbf{u}} \geq 0$, which include contact and (with some modification) dry (Coulomb) friction. At the acceleration level,

these constraints take the form

$$\mathbf{G}(\mathbf{q})\dot{\mathbf{u}} + \mathbf{g} = 0, \quad \mathbf{N}(\mathbf{q})\dot{\mathbf{u}} + \mathbf{n} \geq 0 \quad (1)$$

where \mathbf{g} and \mathbf{n} contain the Coriolis terms $\dot{\mathbf{G}}\mathbf{u}$ and $\dot{\mathbf{N}}\mathbf{u}$. Bilateral and unilateral constraints are enforced, respectively, by Lagrange multipliers $\boldsymbol{\lambda}$ and \mathbf{z} , which generate constraint forces $\mathbf{G}(\mathbf{q})^T\boldsymbol{\lambda}$ and $\mathbf{N}(\mathbf{q})^T\mathbf{z}$. \mathbf{z} is always positive and satisfies a complementarity condition with $\mathbf{N}(\mathbf{q})\dot{\mathbf{u}} + \mathbf{n} \geq 0$. The regular and constraint forces sum to a net force which drives the system according to Newton's second law:

$$\mathbf{M}\dot{\mathbf{u}} = \mathbf{f}(\mathbf{q}, \mathbf{u}, t) + \mathbf{G}(\mathbf{q})^T\boldsymbol{\lambda} + \mathbf{N}(\mathbf{q})^T\mathbf{z}, \quad (2)$$

where \mathbf{M} is a block-diagonal mass matrix. Determining $\dot{\mathbf{u}}$ requires solving (2) together with (1), which can be expressed as a KKT system with inequality constraints,

$$\begin{pmatrix} \mathbf{M} & -\mathbf{G}^T & -\mathbf{N}^T \\ \mathbf{G} & 0 & 0 \\ \mathbf{N} & 0 & 0 \end{pmatrix} \begin{pmatrix} \dot{\mathbf{u}} \\ \boldsymbol{\lambda} \\ \mathbf{z} \end{pmatrix} + \begin{pmatrix} -\mathbf{f} \\ \mathbf{g} \\ \mathbf{n} \end{pmatrix} = \begin{pmatrix} 0 \\ 0 \\ \mathbf{w} \end{pmatrix}, \quad (3)$$

$$0 \leq \mathbf{z} \perp \mathbf{w} \geq 0,$$

where \mathbf{w} is a slack variable. This is equivalent to a mixed linear complementarity problem (LCP) [14].

The system dynamics can be integrated with a variety of integrators, the simplest of which is a symplectic Euler scheme:

$$\mathbf{u}^{k+1} = \mathbf{u}^k + h\dot{\mathbf{u}}^k, \quad \mathbf{q}^{k+1} = \mathbf{q}^k + h\mathbf{Q}\mathbf{u}^{k+1}, \quad (4)$$

where h is the time step size, \mathbf{Q} maps velocities onto $\dot{\mathbf{q}}$ (typically an identity mapping except for rigid bodies), \mathbf{q}^k and \mathbf{u}^k give the values of the state variables at step k , and $\dot{\mathbf{u}}^k$ is determined from by solving (3). This is a first order method that is explicit in \mathbf{u} and implicit in \mathbf{q} . We also provide a higher-order Runge Kutta integrator that calculates $\dot{\mathbf{u}}$ and \mathbf{u} at intermediate trial steps and combines the results.

In situations where the forces are stiff, it is necessary to integrate \mathbf{u} implicitly to avoid the need for extremely small time steps. We can turn (4) into a fully implicit step by replacing $\dot{\mathbf{u}}^k$ with $\dot{\mathbf{u}}^{k+1}$:

$$\mathbf{u}^{k+1} = \mathbf{u}^k + h\dot{\mathbf{u}}^{k+1}. \quad (5)$$

In theory, computing $\dot{\mathbf{u}}^{k+1}$ requires solving (3) with all known quantities estimated for step $k+1$. In practice, since \mathbf{G} and \mathbf{N} often vary slowly and \mathbf{M} is frequently constant, it is usually sufficient to estimate only \mathbf{f} at $k+1$ and to use the other quantities evaluated at k . This amounts to an implicit solve with respect to \mathbf{f} and an explicit solve with respect to \mathbf{G} , \mathbf{N} , etc. Since \mathbf{f}^{k+1} is not known a-priori, we approximate it with a Taylor series expansion:

$$\mathbf{f}^{k+1} \approx \mathbf{f}^k + \frac{\partial \mathbf{f}}{\partial \mathbf{u}} \Delta \mathbf{u} + \frac{\partial \mathbf{f}}{\partial \mathbf{q}} \Delta \mathbf{q}.$$

We also modify (3) so that instead of solving for $\dot{\mathbf{u}}^{k+1}$, we solve directly for $\mathbf{u}^{k+1} = \mathbf{u}^k + h\dot{\mathbf{u}}^{k+1}$. Then, noting that $\Delta \mathbf{q} = h\mathbf{Q}\mathbf{u}^{k+1}$ and $\Delta \mathbf{u} = h\dot{\mathbf{u}}^{k+1}$, and defining

$$\hat{\mathbf{M}} \equiv (\mathbf{M} - h \frac{\partial \mathbf{f}}{\partial \mathbf{u}} - h^2 \frac{\partial \mathbf{f}}{\partial \mathbf{q}} \mathbf{Q}), \quad \hat{\mathbf{f}} \equiv \mathbf{f} - \frac{\partial \mathbf{f}}{\partial \mathbf{u}} \mathbf{u}^k, \quad (6)$$

we obtain the system

$$\begin{pmatrix} \hat{\mathbf{M}} & -\mathbf{G}^T & -\mathbf{N}^T \\ \mathbf{G} & 0 & 0 \\ \mathbf{N} & 0 & 0 \end{pmatrix} \begin{pmatrix} \mathbf{u}^{k+1} \\ \boldsymbol{\lambda} \\ \mathbf{z} \end{pmatrix} + \begin{pmatrix} -\mathbf{M}\mathbf{u}^k - h\hat{\mathbf{f}}^k \\ h\mathbf{g} \\ h\mathbf{n} \end{pmatrix} = \begin{pmatrix} 0 \\ 0 \\ \mathbf{w} \end{pmatrix}, \quad (7)$$

$$0 \leq \mathbf{z} \perp \mathbf{w} \geq 0.$$

1. Find contacts and constraints $\mathbf{G}(\mathbf{q}), \mathbf{N}(\mathbf{q})$.
2. Correct positions \mathbf{q}^k using (8).
3. Update constraints $\mathbf{G}(\mathbf{q}), \mathbf{N}(\mathbf{q})$.
4. Solve for \mathbf{u}^{k+1} (using (7) or equivalent).
5. Adjust velocities \mathbf{u}^{k+1} .
6. $\mathbf{q}^{k+1} = \mathbf{q}^k + h\mathbf{Q}\mathbf{u}^{k+1}$.

Figure 10: Main steps in the ArtiSynth simulation engine.

Here $\boldsymbol{\lambda}$ and \mathbf{z} now give the average constraint impulses over the time step, and the constraints \mathbf{G} and \mathbf{N} are themselves applied directly to the velocity \mathbf{u}^{k+1} , which reduces drift. Solving this system results in a first-order implicit Euler step. By weighting the Jacobian terms with $h/2$ instead of h , the same expression can be used to implement a second order trapezoidal step at no extra cost. By replacing $\hat{\mathbf{M}}$ and $\hat{\mathbf{f}}$ with \mathbf{M} and \mathbf{f} , we obtain an explicit step with the constraint forces applied as impulses. More detailed descriptions of (7), including extensions for dry Coulomb friction, can be found in [1, 13].

Using the Jacobian-modified mass matrix $\hat{\mathbf{M}}$ complicates the solution of (7) because $\hat{\mathbf{M}}$ is no longer block diagonal (although it is still sparse). To solve the system, we use the Pardiso direct sparse solver [15], combined with the Cottle-Dantzig algorithm [14] to handle the LCP associated with the unilateral constraints.

3.2 Simulation Engine Description

We now describe the actual functioning of the ArtiSynth simulation engine. The main steps are described in Figure 10. It has some similarity with the engines described in [16, 6], but is simpler in structure and does not currently use iterative solution methods.

Step 1 begins with collision detection between all colliding bodies (rigid or deformable). Collisions give rise to velocity constraints \mathbf{N} between bodies that serve to prevent further interpenetration, along with interpenetration distances δ_n that need to be corrected in Step 2. Likewise, the constraints \mathbf{G} are determined for bilateral constraints, along with the drift errors δ_g from the constraint surface.

In Step 2, the positions are adjusted so as to remove the interpenetration and drift errors. This is done by computing an impulse $\delta \mathbf{q}$ that corrects the positions while honoring the constraints, using a modified form of (7):

$$\begin{pmatrix} \mathbf{M} & -\mathbf{G}^T & -\mathbf{N}^T \\ \mathbf{G} & 0 & 0 \\ \mathbf{N} & 0 & 0 \end{pmatrix} \begin{pmatrix} \delta \mathbf{q} \\ \boldsymbol{\lambda} \\ \mathbf{z} \end{pmatrix} + \begin{pmatrix} 0 \\ \delta_g \\ \delta_n \end{pmatrix} = \begin{pmatrix} 0 \\ 0 \\ \mathbf{w} \end{pmatrix}, \quad (8)$$

$$0 \leq \mathbf{z} \perp \mathbf{w} \geq 0.$$

This system is easier to solve than (7) because it is usually permissible to use the block-diagonal \mathbf{M} in place of the Jacobian-enhanced $\hat{\mathbf{M}}$.

In Step 3, \mathbf{G} and \mathbf{N} are re-evaluated to reflect the change in \mathbf{q} . We do not perform collision detection again, but rather adjust the collision constraints that were deter-

mined in Step 1. This helps prevent the chattering that can occur if Step 2 removes a collision completely.

Step 4 involves solving for the next-step velocities, using (7) if implicit integration is being used, or a similar formulation for explicit integration.

In Step 5, we apply any needed post-processing to the velocities. If (7) includes all constraints and friction, this is not necessary. However, it is generally more efficient to compute friction separately and apply it as a post-process, which we do here if the associated errors are not too large.

Finally, Step 6 advances the positions using (4).

4. INVERSE MODELING

One significant challenge of forward dynamics simulation is specifying the input muscle activations that produce a desired movement in the dynamic model. We are incorporating inverse modeling methods to automatically predict muscle activations that cause the model to track a target motion trajectory. Our approach is to extend the trajectory tracking algorithm of [19] to work with the full complement of dynamic components in ArtiSynth including muscle-actuated hard and soft tissue structures. The force term in (2) be divided into passive forces \mathbf{f}_p that are uncontrolled and active forces \mathbf{f}_a that arise from muscle actuators:

$$\mathbf{f}(\mathbf{q}, \mathbf{u}, t) = \mathbf{f}_p(\mathbf{q}, \mathbf{u}) + \mathbf{f}_a(\mathbf{q}, \mathbf{u}, \mathbf{a}(t)), \quad (9)$$

where \mathbf{a} is a vector of time-varying muscle activations that lie within the range $[0, 1]$. Commonly used muscle models generate forces that are linear in muscle activation, i.e. $\mathbf{f}_a = \mathbf{A}(\mathbf{q}, \mathbf{u})\mathbf{a}$, where the columns of the \mathbf{A} matrix encode the affect of an individual muscle's force on the total system forces. Given a target acceleration $\dot{\mathbf{u}}^*$, the goal of the inverse solver at each simulation step is to find muscle activations that minimize $\|\dot{\mathbf{u}}^* - \dot{\mathbf{u}}\|^2$. Substituting in (2) and ignoring the constraint terms we have an quadratic programming problem:

$$\begin{aligned} \min_{\mathbf{a}} \quad & \frac{1}{2} \|\dot{\mathbf{u}}^* - M^{-1}\mathbf{f}_p(\mathbf{q}, \mathbf{u}) - M^{-1}\mathbf{A}(\mathbf{q}, \mathbf{u})\mathbf{a}\|^2 + \frac{1}{2} \|\mathbf{a}\|^2 \\ \text{subject to} \quad & 0 \leq \mathbf{a} \leq 1 \end{aligned} \quad (10)$$

Bilateral constraints \mathbf{G} can also be included in this formulation and we are investigating methods to include unilateral constraints \mathbf{N} , although this increases the complexity of the optimization problem.

We are applying these methods to predict muscle activations for jaw-tongue movement as well as hyolaryngeal elevation during swallow using kinematic data from jaw motion tracking or fluoroscopy of the OPAL region. We are also investigating other target parameters such as contact forces and muscle generated stiffness.

5. PROGRESS ON FLUID SIMULATION

We are looking at two different approaches to fluid modeling. First, we use grid-based computational fluid dynamics CFD found in commercial software (Fluent®) based on OPAL geometry modeled in ArtiSynth. Simulations of the bilabial plosive 'pa' have proved to be very useful in understanding this speech utterance. We also applied CFD to the more difficult problem of simulating the acoustics created by turbulence in the fricative consonant 'sh'. Both studies primarily used 3D Large Eddy Simulations

(LES), and demonstrate that this is a promising way to study fluid flow in the vocal tract. The second approach uses an Eulerian approach for modeling liquids that may be appropriate for food bolus modeling [2]. Alternatively, a Lagrangian approach to fluid simulation may be appropriate such as found in [11]. In the future, we would like the link the CFD software with Artisynt to make use of its 3D geometry and investigate fluid structure interactions within the vocal tract.

We are extending the variational framework [2] to the unsteady Stokes problem, in order to solve for the effects of incompressibility and viscosity within a single linear solve. This tighter coupling should reduce splitting errors and hopefully provide speed improvements over existing symmetric indefinite Stokes formulations. Similarly, performing grid refinement studies and analysis will help to understand the spatial accuracy that can be expected, and to understand which weighting schemes provide the most accurate results. We expect these these methods may be adapted to unstructured meshes to enable greater flexibility in the choice of mesh used for simulation and computational resources to be allocated based on importance.

6. APPLICATIONS

The jaw-hyoid model developed to study the biomechanics of chewing [7] can also be used for analyzing functional deficits following surgical resection and reconstruction of the mandible [18]. Typically, these disorders include unstable jaw movements, and difficulties in mastication. They are related to the permanent loss of certain muscles, a compromised articulation, and postoperative scarring. The Artisynt platform is ideal for simulating changes to the muscles driving the jaw, the anatomical substrate (including grafts), and the forces generated by scar tissue (see Figure 1). Moreover, we are able to use both forward and inverse dynamics to study the muscle patterns possible in patients with biomechanically-altered systems. A future development here is the generation of patient-specific models.

We also plan to integrate our present jaw-hyoid model with Artisynt's dynamic tongue, collision-handling for teeth and tongue-palate contact, and the simulation of bolus mechanics. We intend to simulate the entire chewing and swallowing sequence, followed by selective changes to the anatomical structure, its physical properties, and motor drive to the tongue, jaw and pharynx. We believe this will provide insight into the biomechanics of dysphagia, and the peripheral consequences of stroke.

A third application is biomechanical analysis of the jaw's articular function, in particular the functional roles of the lateral pterygoid muscles. Artisynt is highly-suitable for integrating current experimental describing articular structure, dynamic motion of the mandibular condyle, and related muscle activity. Associations among such data suggest a complex relationship between muscle compartmentalization, patterns of muscle activation and biomechanical events. We believe Artisynt is a unique analytical tool for analyzing cause and effect in a region of significant importance to temporomandibular disorders.

7. CONCLUSIONS AND FUTURE WORK

Ultimately, we are seeking to have a protocol that provides medical data acquisition during various behaviours

such as respiration, eating and speaking to help diagnosis and treat deficits as well as increase our understanding of the OPAL complex. Our modeling efforts begin with various image processing techniques applied to MR and CT scans that allow us to create meshes modeling morphology of various OPAL structures. We intend to continue to improve our techniques to minimize the degree of human intervention and to be robust when performing automatically. We intend to extend the types of data we can capture including force profiles during mastication and swallowing, EMG data during various behaviours and elastography of the various tissues to provide estimates of the material properties for better modeling.

ArtiSynth continues to expand to meet the challenges of modeling the OPAL complex. We expect to add non-linear constituent equations into the FEM formulation to provide additional fidelity for improving accuracy of our soft/hard tissue simulations. We are documenting and refactoring the ArtiSynth code base to make it more accessible to non-programmers.

Our fluid modeling of the OPAL complex is just starting, but our results are promising. We require a simpler method to extract vocal tract geometry to interface with software outside ArtiSynth such as Fluent® to leverage existing tools when performing decoupled simulations of fluid. We intend to include a Lagrangian approach to food bolus modeling which will require a remeshing algorithm to be included in ArtiSynth for stable simulation. The fluid models will need to be validated against real data.

Finally, the tools and data currently available have allowed us to model some mastication disorders associated with jaw graft. This work is leading to new insights as to the role of scarring and muscle loss in contributing to post-surgical efficacy. We plan to acquire more data to help model tissue properties as well as kinematic and force data to help validate the accuracy of our models. We are also investigating swallowing disorders using the same approach as for mastication modeling.

Collectively, the OPAL research group is making progress on all fronts of modeling the OPAL complex for medical and scientific applications. We encourage researchers to participate in the development of models inside of ArtiSynth to provide a common platform for our community to construct deeper understandings of the nature of the oral, pharyngeal and laryngeal complex. The OPAL website is at: www.magic.ubc.ca/OPAL.htm and the ArtiSynth software is at www.artisynth.org.

8. REFERENCES

- [1] ANITESCU, M., AND POTRA, F. A. A time-stepping method for stiff multibody dynamics with contact and friction. *International Journal for Numerical Methods in Engineering* 55, 7 (Nov. 2002), 753–784.
- [2] BATTY, C., AND BRIDSON, R. Accurate viscous free surfaces for buckling, coiling, and rotating liquids. In *Eurographics/ACM SIGGRAPH Symposium on Computer Animation* (2008), p. to appear.
- [3] BOOKSTEIN, F. L. Principal warps: Thin-plate splines and the decomposition of deformations. *IEEE Transactions on Pattern Analysis and Machine Intelligence* 11, 6 (1989), 567–585.
- [4] CHAN, T., AND VESE, L. Active contours without edges. *IEEE Trans on Image Processing* 10, 2 (2001), 266–277.
- [5] GERARD, J., PERRIER, P., AND PAYAN, Y. *3D biomechanical tongue modelling to study speech production*. Psychology Press: New-York, USA, 2006, pp. 85–102.
- [6] GUENDELMAN, E., BRIDSON, R., AND FEDKIW, R. Nonconvex rigid bodies with stacking. In *SIGGRAPH '03: ACM SIGGRAPH 2003 papers* (2003), pp. 871–878.
- [7] HANNAM, A., STAVNESS, I., LLOYD, J., AND FELLS, S. A dynamic model of jaw and hyoid biomechanics during chewing. *J Biomechanics* 41, 5 (2008), 1069–1076.
- [8] IRVING, G., SCHROEDER, C., AND FEDKIW, R. Volume conserving finite element simulations of deformable models. In *SIGGRAPH '07: ACM SIGGRAPH 2007 papers* (2007), p. 13.
- [9] LIU, L., BAJAJ, C., DEASY, J. O., LOW, D. A., AND JU, T. Surface reconstruction from non-parallel curve networks. *Eurographics* 27, 2 (2008), 155–163.
- [10] MAES, F., COLLIGNON, A., VANDEERMEULEN, D., MARCHAL, G., AND SUETENS, P. Multimodality image registration by maximization of mutual information. *IEEE Trans. in Medical Imaging* 16 (1997), 187–198.
- [11] NICOSIA, M. A planar finite element model of bolus containment in the oral cavity. *Computers in Medicine and Biology* (2007), in press.
- [12] POON, M., HAMARNEH, G., AND ABUGHARBIH, R. Efficient interactive 3d livewire segmentation of complex objects with arbitrary topology. *Comput. Med Imaging and Graphics* (2009), in press.
- [13] POTRA, F. A., ANITESCU, M., GAVREA, B., AND TRINKLE, J. A linearly implicit trapezoidal method for integrating stiff multibody dynamics with contact, joints, and friction. *International Journal for Numerical Methods in Engineering* 66, 7 (2006).
- [14] RICHARD W. COTTLE, JONG-SHI PANG, R. E. S. *The Linear Complementarity Problem*. Academic Press, 1992.
- [15] SCHENK, O., AND GÄRTNER, K. Solving unsymmetric sparse systems of linear equations with pardiso. *Future Gener. Comput. Syst.* 20, 3 (2004), 475–487.
- [16] SHINAR, T., SCHROEDER, C., AND FEDKIW, R. Two-way coupling of rigid and deformable bodies. In *SCA '08: Proceedings of the 2008 ACM SIGGRAPH/Eurographics Symposium on Computer Animation* (2008).
- [17] SLED, G., ZIJDENBOS, A. P., AND EVANS, A. C. Non-parametric method for automatic correction of intensity nonuniformity in mri data. *IEEE Trans. in Medical Imaging* 17, 1 (1998), 87–97.
- [18] STAVNESS, I., HANNAM, A. G., LLOYD, J. E., AND FELLS, S. Towards predicting biomechanical consequences of jaw reconstruction. *IEEE Engineering in Medicine and Biology Society Conference* (2008), 4567–4570.
- [19] SUEDA, S., KAUFMAN, A., AND PAI, D. K. Musculotendon simulation for hand animation. In *SIGGRAPH '08: ACM SIGGRAPH 2008 papers* (New York, NY, USA, 2008), ACM, pp. 1–8.
- [20] THEVENAZ, P., AND UNSER, M. An efficient mutual information optimizer for multiresolution image registration. In *Proc. of ICIP* (1998), pp. 833–837.
- [21] TRUCCO, E., FUSIELLO, A., AND ROBERTO, V. Robust motion and correspondence of noisy 3-d point sets with missing data. *Pattern Recog Lett* 20, 9 (1999), 889–898.
- [22] UMEYAMA, S. Least-squares estimation of transformation parameters between twopoint patterns. *IEEE Transactions on Pattern Analysis and Machine Intelligence* 13, 4 (1991), 376–380.
- [23] VIOLA, P., AND III, W. M. W. Alignment by maximization of mutual information. In *Proc of ICCV* (1995), pp. 16–23.
- [24] VOGT, F., LLOYD, J. E., BUCHAILLARD, S., PERRIER, P., CHABANAS, M., PAYAN, Y., AND FELLS, S. S. Investigation of efficient 3D finite element modeling of a muscle-activated tongue. *Proceedings of ISBMS 06 in Springer LNCS 4072* (2006), 19–28.
- [25] WANG, X., CHENG, Y.-Q., COLLINS, R. T., AND HANSON, A. R. Determining correspondences and rigid motion of 3-d point sets with missing data. In *Proc. of CVPR* (1996), pp. 252–257.